MEMORIAL UNIVERSITY

Synthetic modelling of marine controlled-source electromagnetic data for hydrocarbon exploration

Mariella Nalepa, SeyedMasoud Ansari, and Colin Farquharson
Department of Earth Sciences, Memorial University of Newfoundland, St. John's, Newfoundland, Canada

GeoConvention Calgary • Canada • March 7-11 2016
OPTIMIZING RESOURCES

The marine CSEM method

The marine CSEM method is a geophysical technique for mapping subsurface resistivity structure in the offshore environment through measurement of the electric and magnetic fields arising from excitation of the earth by a controlled source.

It serves as an independent yet complementary method to the seismic reflection method for hydrocarbon exploration due to the strong dependence of bulk rock resistivity on pore fluid content, e.g., conductive seawater versus resistive oil or gas.

Conventional acquisition employs a horizontal electric dipole source which transmits a low-frequency, broadband EM signal into the earth (**Figure 1**), where it is modified in amplitude and phase via interactions with the earth's electrical structure.

Measurements of the fields at receivers placed at the seafloor can be related back to variations in the earth's electrical structure through **modelling.**

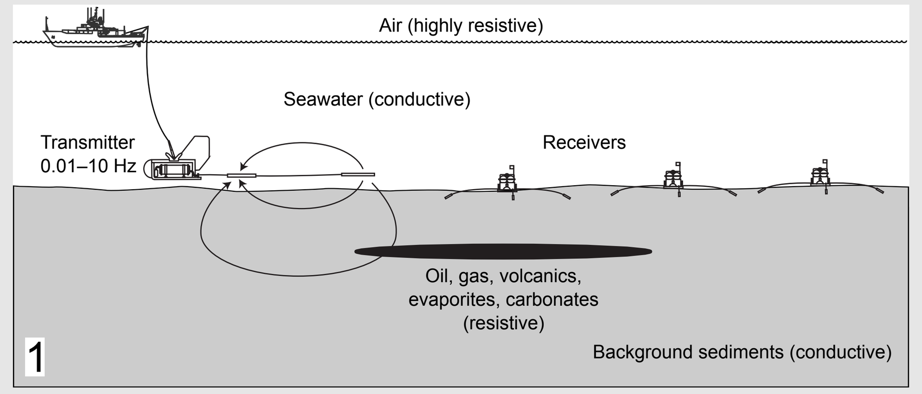

Figure 1 Illustration of the marine CSEM method. The transmitter is towed close to the seafloor to maximize coupling of the electric field to the subsurface. A horizontal electric dipole source excites vertical currents transverse to horizontal resistive targets, thereby generating a galvanic perturbation in the electric field which may be detected at the seafloor surface. Modified from Constable and Weiss (2006).

Motivation

Growing application of the CSEM method has motivated the development and advancement of software for CSEM interpretation and integration.

For arbitrary 2D or 3D earth models, numerical methods, such as the finite-difference or **finite-element** methods, are required for solution of the CSEM forward problem.

This work contributes to the ongoing development of the **3D CSEM finite-element code of Ansari et al. (2015; also Ansari and Farquharson, 2014)**, which has had limited application to marine sedimentary models and more realistic models in general.

To address the challenges of incorporating realistic structural elements (e.g., finite and irregular subsurface bodies, topographic or straitgraphic surfaces) in a geoelectric model to be discretized using unstructured meshes, a suite of models of progressive structural complexity were examined.

The ultimate goal of this work was to synthesize CSEM data for a real-world-based model for practical application, e.g., feasibility studies to assess the utility of CSEM data for specific offshore hydrocarbon exploration and development scenarios.

Methodology

Vector-scalar potential problem formulation

The electric field **E** is decomposed into the vector magnetic potential **A** and scalar electric potential ϕ to avoid the numerical instability of the electric field formulation at low frequency:

$$\nabla \times \nabla \times \mathbf{E} + i\omega\mu_0\sigma\mathbf{E} = -i\omega\mu_0\mathbf{J}_\mathbf{e}^\mathbf{s}$$

$$\mathbf{E} = -i\omega\mathbf{A} - \nabla\phi$$

$$\nabla \times \nabla \times \mathbf{A} + i\omega\mu_0\sigma\mathbf{A} + \mu_0\sigma\nabla\phi = \mu\mathbf{J}_\mathbf{e}^\mathbf{s}$$

$$-i\omega\nabla\cdot(\sigma\mathbf{A}) - \nabla\cdot(\sigma\nabla\phi) = -\nabla\cdot\mathbf{J}_\mathbf{e}^\mathbf{s}$$

Finite-element discretization on unstructured meshes

The computational domain is divided or ***discretized*** into subdomains (cells, elements).

The finite-element method is readily applied to boundary-conforming unstructured meshes which enable more accurate representation of complex structure than rectilinear meshes (compare **Figures 2a** and **2b**), as well as locally-restricted cell refinement, i.e., cell dimensions do not propagate through the mesh (compare **Figures 2c** and **2d**). The TetGen software package (Si, 2015) was employed in this study for unstructured mesh generation.

The vector and scalar potentials are expressed as expansions in a finite number of of vector and scalar basis functions associated with the element edges and nodes (**Figure 3**):

$$\mathbf{A} = \sum_{j=1}^{n_A} A_j\mathbf{N}_j \qquad \phi = \sum_{k=1}^{n_\phi} \phi_k N_k$$

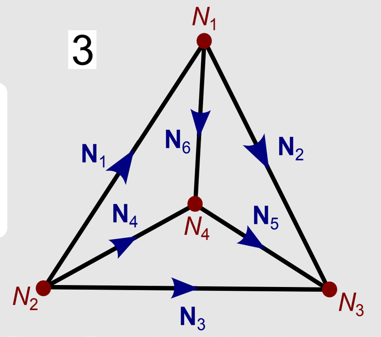

Figure 3 Tetrahedron with basis function associations to edges and nodes illustrated.

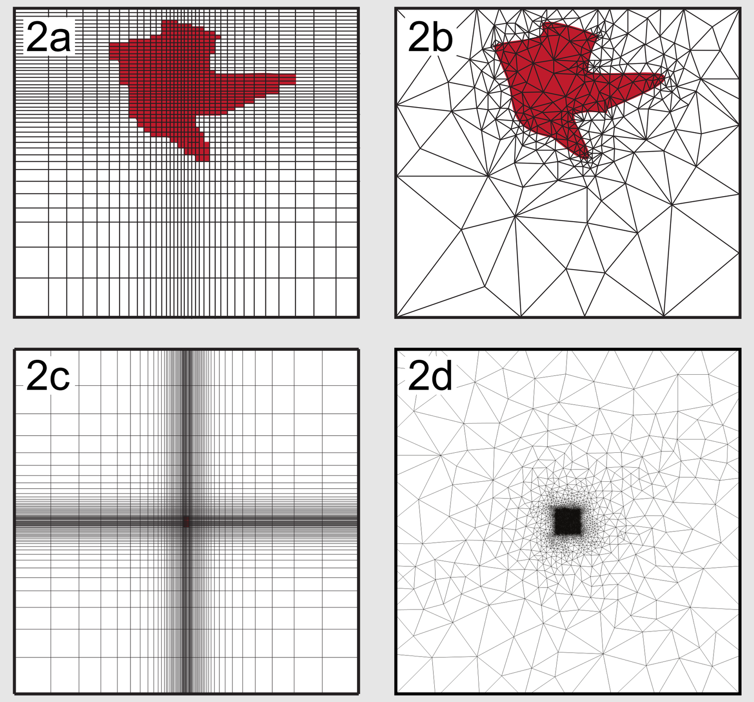

Figure 2 Discretization using structured rectilinear meshes versus unstructured tetrahedral meshes. **(a)** Structured mesh for an irregular body. **(b)** Equivalent unstructured mesh for the same irregular body. **(c)** Structured mesh where refinement at the centre of the mesh requires small cell dimensions that extend to the boundaries of the mesh. **(d)** Equivalent unstructured mesh where small cells for refinement are localized to the centre of the mesh.

Challenges

Generation of unstructured meshes of suitable quality for numerical solution of PDE problems is non-trivial and an area of ongoing research.

Mesh quality is a complex function of mesh geometry, including cell size and shape, and effects the accuracy of the numerical solution in terms of discretization and interpolation errors, as well as the conditioning of the stiffness matrix (Shewchuk, 2002; Du et al., 2009; Si, 2015).

Iterative solution methods are implemented instead of direct solution methods because of the lower memory requirements. The disadvantage of iterative methods is that their performance is more sensitive to system ill-conditioning.

1.0 Canonical disk model

Uniform-thickness, laterally-finite petroleum reservoir

The canonical disk model (Constable and Weiss, 2006) is a 3D adaptation of the 1D canonical oil field model inspired by the Girassol oil field located offshore Angola, which was the location for the first CSEM field trial by the oil and gas industry (Ellingsrud et al., 2002; Constable, 2010).

The model consists of a variable-diameter buried disk that is representative of a laterally-terminating, uniform-thickness petroleum reservoir **(Figures 4 and 5)**.

Results demonstrate the edge effects of laterally-finite resistive layers on the CSEM response: for offsets less than the disk diameter, the 3D finite-element solution follows the 1D solution for an infinite-extent resistive layer, but for offsets greater than the disk diameter, the 3D solution falls below the 1D resistive layer solution and exhibits the same exponential decay as the 1D homogeneous halfspace solution (i.e., no disk, or resistive hydrocarbons, present) in its asymptotic limit **(Figure 6)**.

The 1 km-diameter disk at a burial depth of 1 km is essentially invisible to the CSEM method with less than a 20% difference in amplitude relative to the homogeneous halfspace.

1D modelling can only provide a best-case, upper estimate of the response for a finite-extent target.

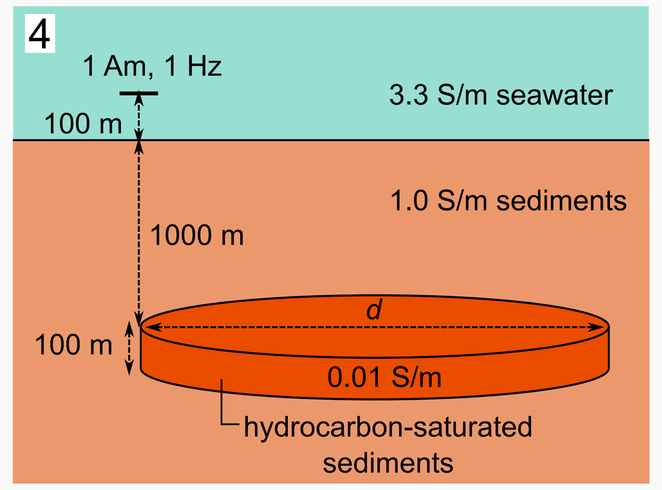

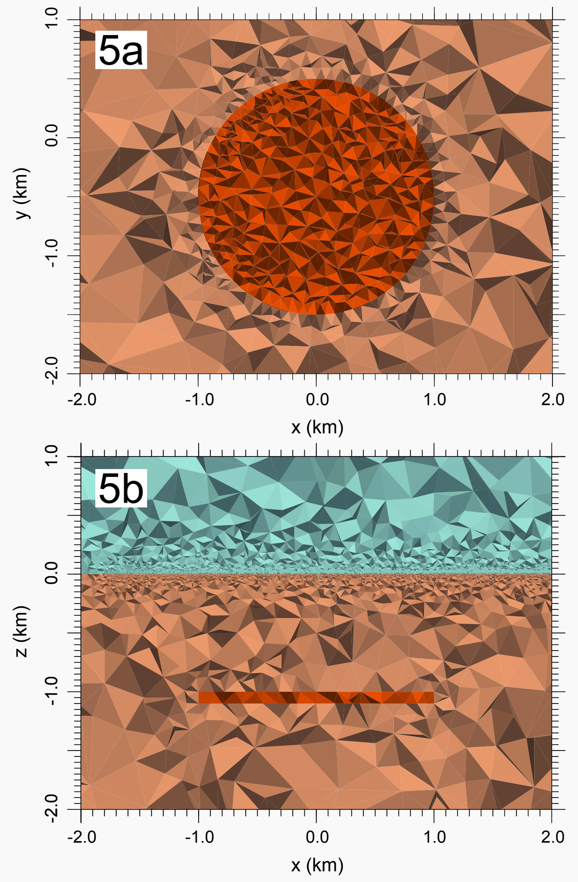

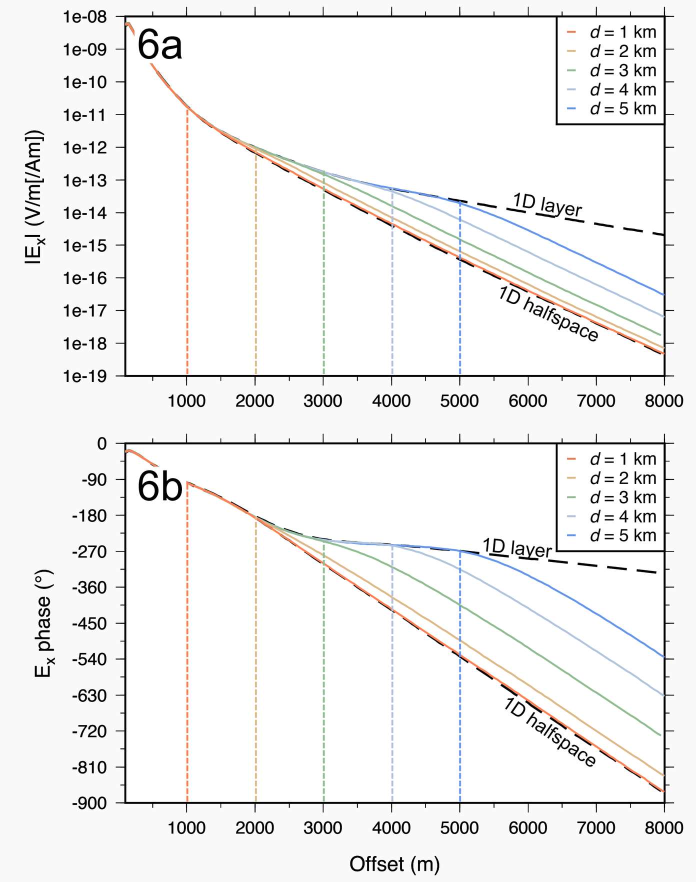

Figure 4 Schematic of the canonical disk model, which consists of a variable-diameter, 100 m-thick, 0.01 S/m (100 ohm-m) disk buried at a depth of 1 km within a 1 S/m (1 ohm-m) homogeneous sediment halfspace with an overlying 3.3 S/m (0.3 ohm-m) sea halfspace.

Figure 5 (a) *xy*(depth)- and **(b)** *xz*(cross)-sections of the unstructured mesh for the 2 km-diameter disk model.

Figure 6 Dipole moment-normalized inline electric field **(a)** amplitude and **(b)** phase for various disk diameters *d*. The 1D solutions for an equivalent-thickness, infinite-extent layer and a homogeneous halfspace (i.e., no resistive layer present) are also plotted for comparison.

2.0 Inclusion of seafloor topography

An irregular surface was introduced as the interface between a lower sediment and upper sea halfspace to study the effects of topography on the CSEM response.

Seafloor topography was based on the 'mmal25pm' mesh available from the INRIA Gamma Group 3D mesh research database (**Figure 7**). This mesh was previously used in the seafloor topography model presented by Schwarzbach et al. (2011).

Results indicate that the CSEM response in the presence of laterally-variable topography, and therefore resistivity, substantially deviates from the CSEM response for a flat seafloor model (**Figure 8**).

To avoid artefacts in interpretation of real CSEM data, geoelectric models should ideally include topography, especially when considering regions of substantial topographic relief.

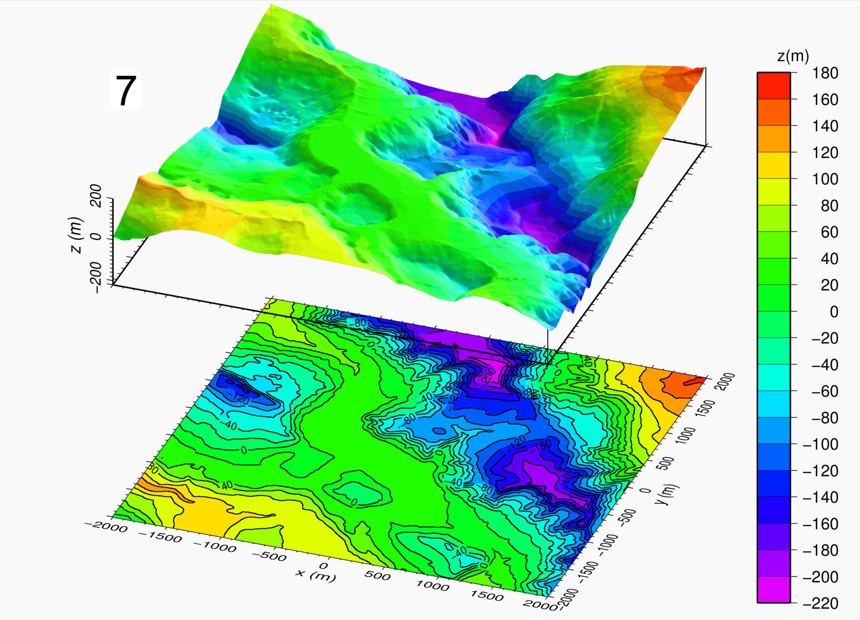

Figure 7 Topographic mesh 'mmal25pm', available from the INRIA mesh database, that was used for construction of the seafloor topography model.

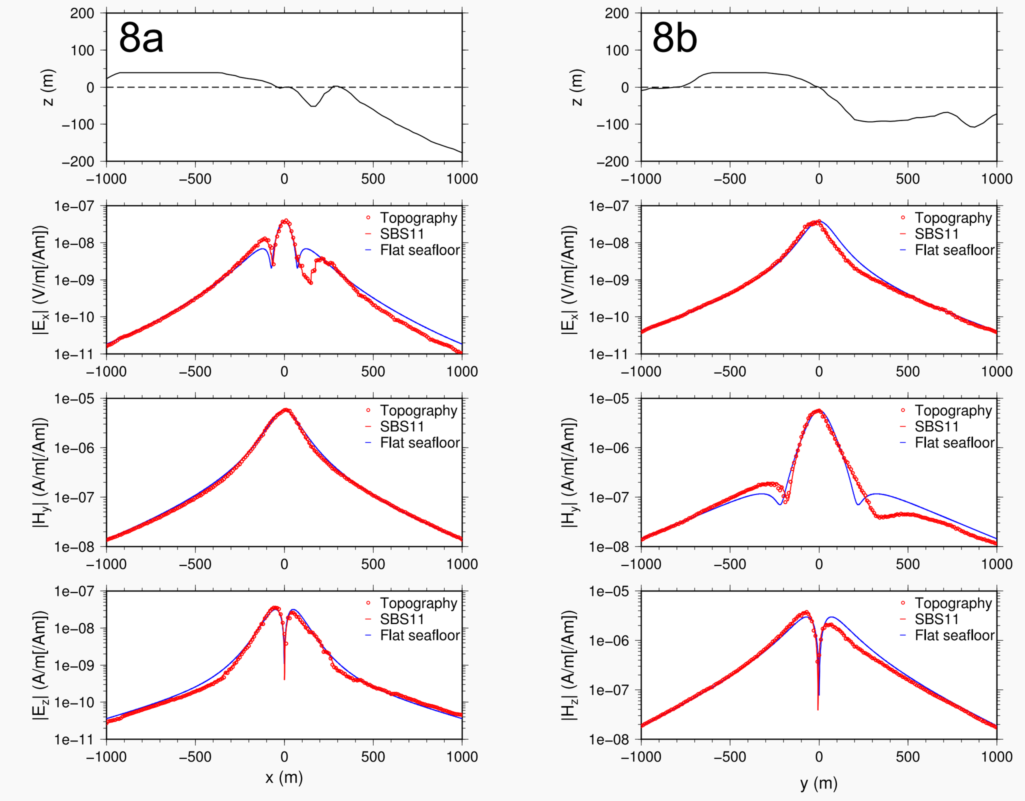

Figure 8 Dipole moment-normalized amplitudes for the non-vanishing inline electric and magnetic field components for **(a)** an *x*-profile and **(b)** a *y*-profile through the seafloor topography model. The topographic profiles are shown in the top panels.The 1D field solutions for a flat seafloor are plotted for comparison, as well as the finite-element seafloor topography solution of Schwarzbach et al., (2011; in legend, SBS11).

3.0 Marine reservoir model

Based on the North Amethyst oil field, Jeanne d'Arc Basin, offshore Newfoundland

A simplified 3D reservoir model was constructed for the North Amethyst field using resistivity logs and seismic horizons. The 3D model simplifies stratigraphy and associated resistivity structure to a reservoir embedded within a shale halfspace with an overlying 120 m-thick sea layer and upper air halfspace (**Figure 9**).

Preliminary 1D modelling suggests that simplification of background structure does not significantly modify the frequency-offset field for anomaly detection (0.01–0.1 Hz; offset greater than 5 km), but does result in overestimation of anomaly magnitude (**Figure 10**).

Simulated 3D CSEM data (**Figure 11a**, 'True Model') suggests that the North Amethyst reservoir modelled here is not a favourable target for detection via the marine CSEM method, likely due to the combination of its significant burial depth, limited lateral extent, and location in shallow water.

For increased water depth, decreased burial depth, and/or increased hydrocarbon content, the electric field anomaly increases, underscoring the sensitivity of the method to transverse resistivity (resistivity-thickness product) and its suitability to the deep water environment (**Figure 11**).

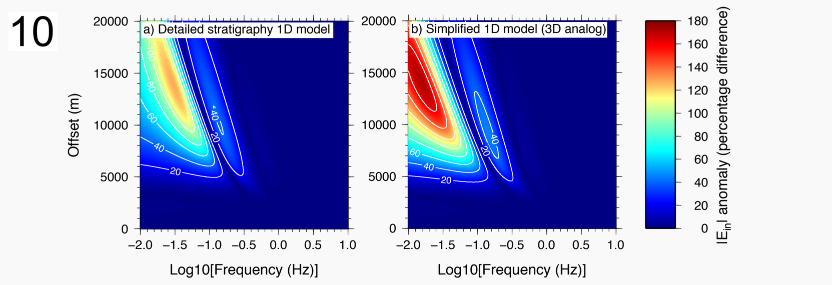

Figure 10 Horizontal inline electric field anomalies as a function of frequency and offset for **(a)** the 1D model with detailed stratigraphy derived from resistivity logs, and **(b)** the 1D model of a shale halfspace containing an infinite-extent reservoir.

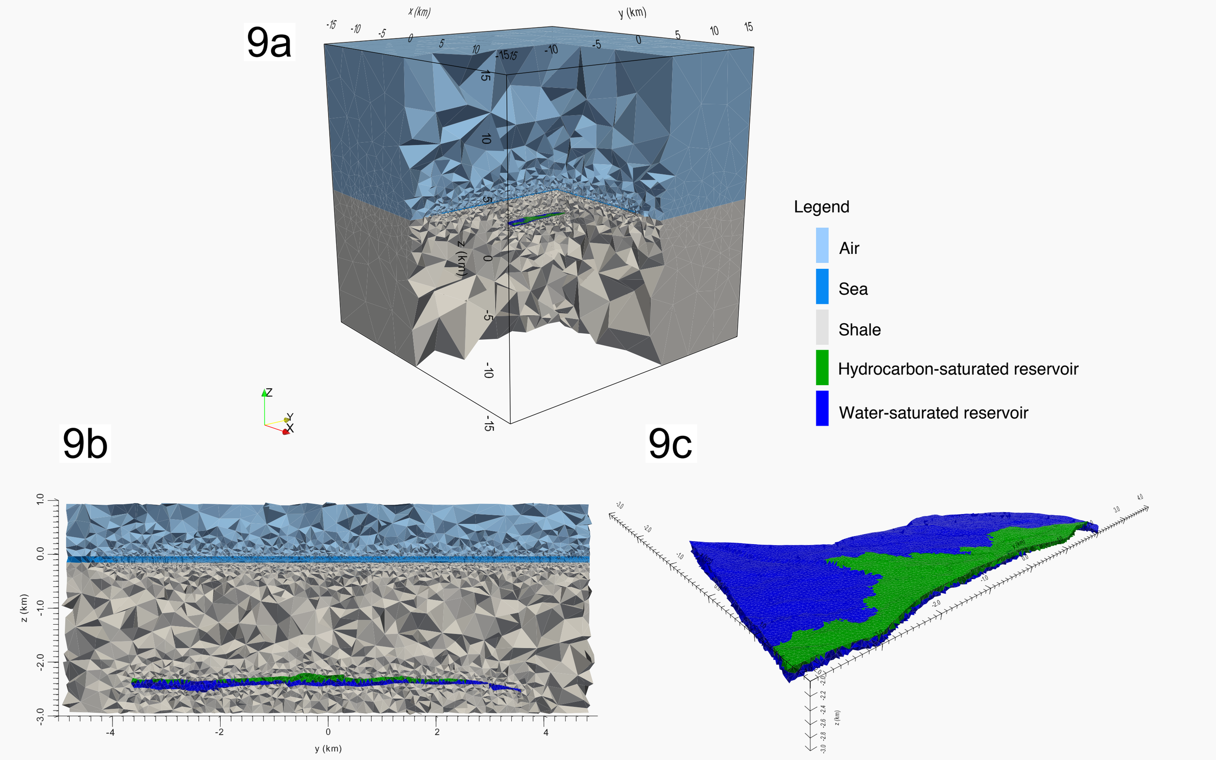

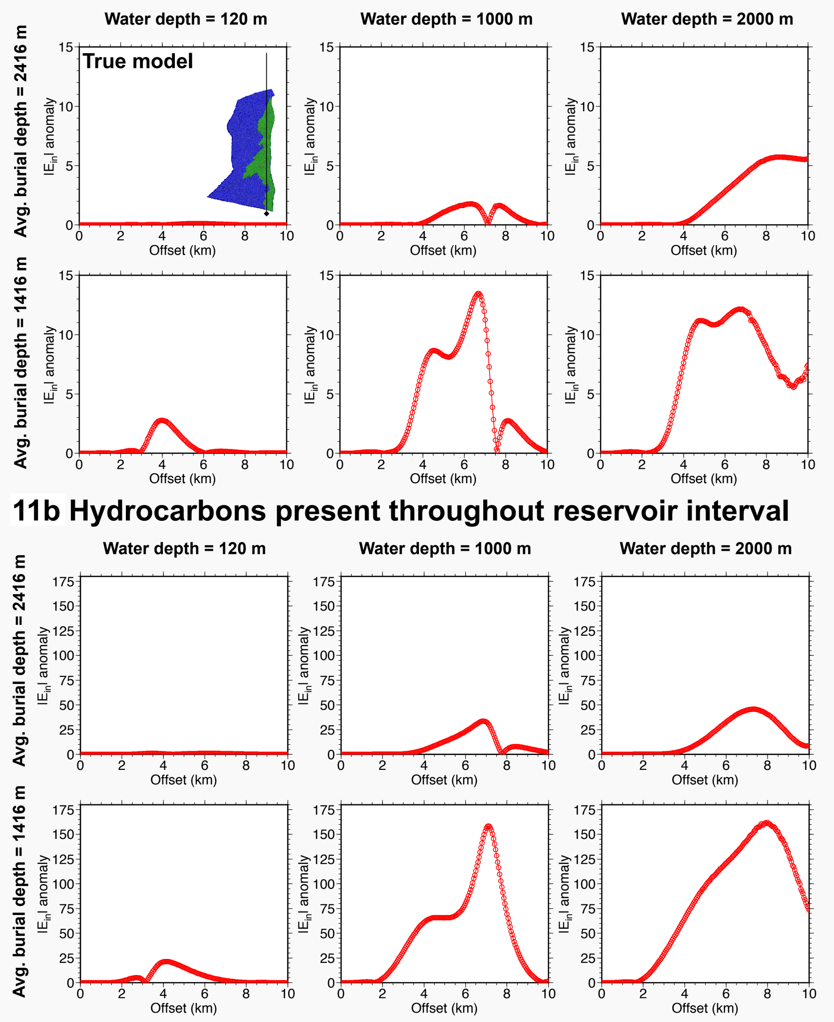

Figure 9 Unstructured mesh for the 3D North Amethyst reservoir model, where **(a)** illustrates a cut-out of the mesh for the full model domain, **(b)** illustrates an *xy*-section through the reservoir interval, and **(c)** illustrates the meshed reservoir interval in isolation.

Figure 11 Inline horizontal electric field anomaly as a function of offset for variations of the baseline (true) 3D North Amethyst model in terms of water depth and reservoir burial depth, for **(a)** the scenario of true hydrocarbon content, i.e., hydrocarbons above the oil-water contact only, and **(b)** the scenario of the reservoir interval being completely hydrocarbon-filled. Note the change in scale from 0-15% in (a) to 0-200% in (b). The source-receiver line, inline with the hydrocarbon trend, is shown inset in the upper left plot of (a).

Conclusions

The accuracy of the CSEM3DFWD code has been verified for several simple earth models for which 1D or other numerical 3D solutions exist. Notably, the forward code has been demonstrated to accurately simulate CSEM data for models featuring finite-depth sea and infinite air layers, scenarios which had not previously been tested.

To the authors' knowledge, the North Amethyst reservoir model presented here represents one of the few examples in the 3D EM modelling literature of discretization of a realistic 3D model using unstructured meshes.

Unstructured meshes have been demonstrated to accurately represent realistic and complex structure, but implementation of FE schemes on unstructured meshes remains computationally challenging, in particular for models featuring thin layers and/or fine structural detail.

In the future, it may be advantageous to explore schemes which automate and optimize mesh generation, alternative preconditioning measures to improve the condition number of the stiffness matrix prior to solution, and domain decomposition procedures to reduce problem size and enable parallelization.

Acknowledgements

The authors would like to thank Ayiaz Kaderali, Jim Anstey, and Greg Molloy for their advice and encouragement in this project, Dr. Peter Lelièvre for providing essential model-building software and mesh and data manipulation programs, and Dr. Christoph Schwarzbach for providing and permitting the use of his finite-element solutions for the seafloor topography model.

References

Ansari, S., and C. G. Farquharson, 2014, 3D finite-element modeling of electromagnetic data using vector and scalar potentials and unstructured grids: Geophysics, **79**, no. 4, E149-E165.
Ansari, S., C. G. Farquharson, and S. MacLachlan, 2015, Gauged vector finite-element schemes for the geophysical EM problem for unique potentials and fields: 85th Annual International Meeting, SEG Expanded Abstracts, 801-805.
Constable, 2010, Ten years of marine CSEM for hydrocarbon exploration: Geophysics, **75**, no. 5, 75A67-75A81.
Constable, S. C., and C. J. Weiss, 2006, Mapping thin resistors and hydrocarbons with marine EM methods: Insights from 1D modeling: Geophysics, **71**, no. 2, G43-G51.
Du, Q., D. Wang, and L. Zhu, 2009, On mesh geometry and stiffness matrix conditioning for general finite element spaces: Society for Industrial and Applied Mathematics Journal on Numerical Analysis, **47**, no. 2, 1421-1444.
Ellingsrud, S., T. Eidesmo, S. Johansen, M. C. Sinha, L. M. MacGregor, and S. Constable, 2002, Remote sensing of hydrocarbon layers by seabed logging (SBL): Results from a cruise offshore Angola: The Leading Edge, **21**, no. 10, 972-982.
Schwarzbach, C., R.-U. Börner, and K. Spitzer, 2011, Three-dimensional adaptive higher order finite element simulation for geoelectromagnetics — a marine CSEM example: Geophysical Journal International, **187**, no. 1, 63-74.
Shewchuk, J. R., 2002, What is a good linear finite element? Interpolation, conditioning, anisotropy, and quality measures: Technical Report, Department of Computer Science, University of California at Berkeley. *Available at http://www.cs.berkeley.edu/~jrs/jrspapers.html*.
Si, H., 2015, TetGen, a Delaunay-based quality tetrahedral mesh generation: ACM Transactions on Mathematical Software, **41**, no. 2, article no. 11, 36 pages.

Contact emails: Mariella Nalepa, mnalepa@mun.ca; SeyedMasoud Ansari, seyedmasoud.ansari@mun.ca; Colin Farquharson, cgfarquh@mun.ca